

Research Article

Computational Study on the Photovoltaic Properties of Thiazole-Based Acceptors in Fullerene-Free Organic Solar Cells: A Theoretical Approach

Neelam Shahzadi , Iqra Naz* , Rehmat Illahi

Department of Chemistry, University of Education, Lahore, Pakistan

Abstract

A promising approach to enhance the power conversion efficiency of organic solar cells (OSCs) is end-capped group reconfiguration. Five distinct acceptor molecules were produced by end-group modification of the recently synthesized chemical DC-IDT2Tz (R). Density functional theory (DFT) and time-dependent DFT were utilised for computing an array of geometric and photovoltaic features of formulated and reference molecules, consisting of charge transfer analysis, the energy of excitation, absorption maximum, binding energy, oscillator strength, frontier molecular orbital analysis, and transition density matrix analysis. The absorption spectra of newly designed compounds exhibited a narrow energy band gap (E_g) with red-shifting. Engineered chemicals additionally demonstrate lower binding and excitation energies. A comprehensive investigation is conducted as well to assess the charge transfer between the acceptor and donor parts. The aforementioned investigations indicated that the discovered chemicals possess intriguing potential for optimized organic solar cell implementation. The modification of terminal structures has been revealed to be effective in modifying the energy levels of frontier molecular orbitals, band gap, absorption spectra, reorganization energy, open-circuit voltage, and binding energy values in the inspected molecules. In light of the above results, these compounds show potential as acceptor materials.

Keywords

Time-Dependent Density Functional Theory, Fullerene-free Organic Solar Cell, Frontier Molecular Orbitals Analysis, Transition Density Matrix, Oscillator Strength, Molecular Electric Potential

1. Introduction

The depletion of non-renewable energy resources over time has led to environmental pollution [1]. In order to meet the growing energy demand, alternative forms of energy like hydroelectric plants and wind power mills have been explored [2]. The discovery of solar cells in the 19th century revolutionized the utilization of sunlight, the primary source of energy on Earth [3]. Solar cells convert photons into electrical

energy through the photovoltaic effect [4]. Fullerene derivatives have historically been a vital part of OSCs as electron acceptor [5-7]. However, constraints of fullerene derivatives such as poor light absorbance, film stiffness, limited tunability and increasing purifying costs act as a barrier to further enhancing the efficiency and various functionalities of OSCs [8-10]. Consequently, there is an urgent need to develop

*Corresponding author: Iqran2756@gmail.com (Iqra Naz)

Received: 04 January 2025; Accepted: 17 March 2025; Published: 22 May 2025



Copyright: © The Author(s), 2025. Published by Science Publishing Group. This is an **Open Access** article, distributed under the terms of the Creative Commons Attribution 4.0 License (<http://creativecommons.org/licenses/by/4.0/>), which permits unrestricted use, distribution and reproduction in any medium, provided the original work is properly cited.

novel acceptors [11-13]. Many current attempts are being made to reach efficiencies of more than 12% for fullerene-free OPVs [14-16].

There has always been a lot of attention and quick progress in the creation of organic solar cells (OSCs) that use non-fullerene acceptors (NFAs) lately. [17]. The advancements in donor and NFA designs, along with device optimization, have contributed to the increased PCE of OSCs [18]. Symmetrically structured aromatic compounds play a crucial role in the development of NFAs. These NFAs offer several advantages for instance efficient Intramolecular transfer of charges, wide absorption and a molecular hands-on configuration. Consequently, they have a frequent role as donor components in small-molecule NFAs.

Indaceno [2,1-b:6,5-b]dithiophene (IDT) and 1,1-dicyanomethylene-3-indanone (DC) based NFAs are considered as auspicious age of NFAs. Intermolecular relations and solubility of the intended molecule are governed by four hexylphenyl groups on the outside locations of the plane backbones and the coplanar and rigid construction of IDT is favorable for charge transfer [10, 20]. On the other hand, DC

has a great propensity to pull electrons, which results in low energy levels [21]. Because of this combination, the acceptor exhibits a deep energy level, a powerful, remarkable and expanded spectrum absorption, a tiny bandgap and optimum electronic movement. A small molecular NFA, DC-IDT2Tz, was designated by Zhou et al having IDT core and DC terminal groups alongside thiazole π -bridge [22].

In this study, we reveal five NFA molecules NS1, NS2, NS3, NS4 and NS5 with reduced band gaps in addition to elevated charge mobilities when compared to the reference molecule DC-IDT2Tz illustrated in Figure 1. The aforementioned created molecules were constructed from the molecular structure of DC-IDT2Tz while previously announced novel acceptor groups showed improved photovoltaic parameters. Such acceptor moieties have the ability to broaden the absorption range, whereas the thiazole bridge also contributes to transfer of charges from the center to the terminal acceptor. The mentioned molecules (NS1-NS5) have been shown to be far more effective as an active layer in OSCs in comparison to DC-IDT2Tz molecule.

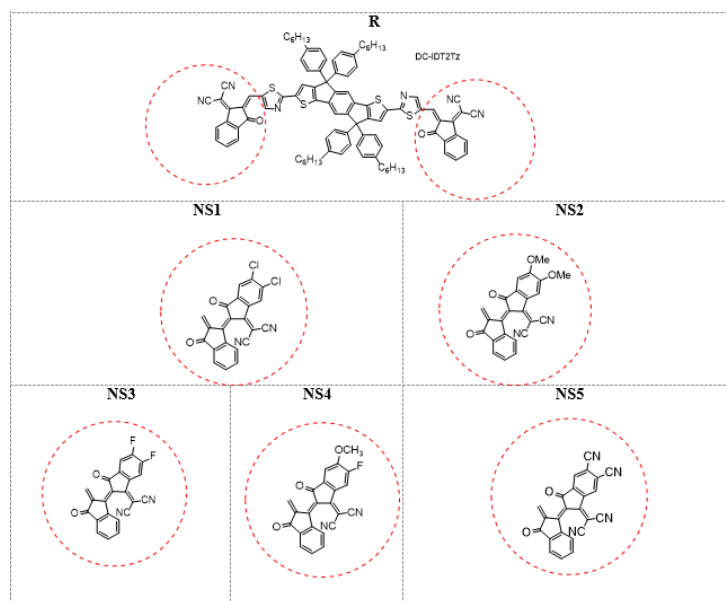


Figure 1. Two dimensional morphologies of Reference and altered acceptors NS1-NS5.

2. Computational Details

Theoretical computations and visualization of the researched molecules' geometry were performed using Gaussian 09 [23] and GaussView 5.0 [24] software, respectively. Density functional theory (DFT) was implemented to estimate the electrical, vibrational and thermodynamic parameters [25].

Initially, The ground state of the reference molecule was optimised by making use of four primary functionals: B3LYP

[26], MPW1PW91 [29], CAM-B3LYP [27, 28] and wB97XD [29], by means of the 6-31G (d,p) basis set. The optimization was carried out under default spin conditions via DFT. Subsequently, by applying time-dependent analysis DFT (TD-DFT), the excited state characteristics of the reference molecule incorporating these functionals were investigated. This allowed for the analysis of electronic properties and transitions of molecule in its excited state.

The effect of the solvent was examined by implementing the CPCM in chloroform [30]. IEPCM accounts for impact of the solvent on electronic traits of molecules.

To determine λ_{\max} , the obtained data was processed using the Swizard program. Subsequently, the λ_{\max} values were plotted using Origin 6.0 [31, 32] software.

The optoelectric properties of freshly created molecular configurations were assessed by analysing their energy gaps, frontier molecular orbitals (FMOs) and density of states (DOS) and transition density matrix (TDM) and charge mobilities and contrasting them with the reference (R). DOS (as analysed by PyMOLyze software program) describes radia-

tion absorption by distinct fragments of a molecule [33]. Marcus' idea [34] described the effective charge transfer.

The reference R's λ_{\max} values in the solution phase were checked against the practical λ_{\max} values via all aforementioned four functionals. (Figure 2). B3LYP provided the greatest λ_{\max} value (733nm) than the experimental value (666nm), proactively making us to believe that It is the finest match. The reference molecule's band gap with B3LYP functional was better than the experimental band gap.

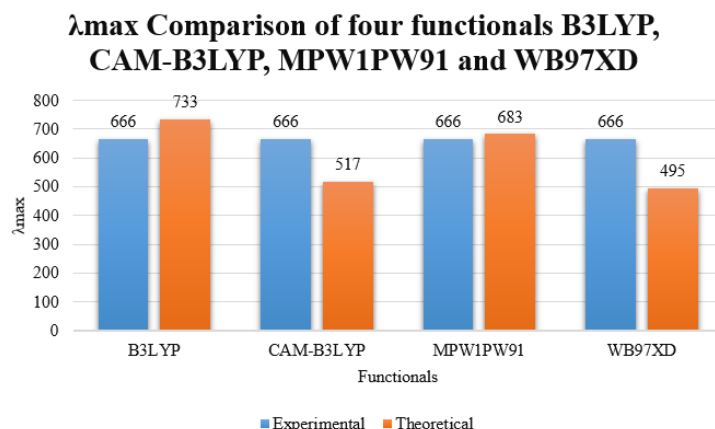


Figure 2. λ_{\max} comparison of experimental and theoretical values of R at 4 functionals.

The λ_{\max} values obtained from all the equations were analyzed and compared to determine the functional that best matched the reference molecule's absorption characteristics.

$$\lambda_e = [E_0^- - E^-] + [E_0^0 - E_0] \quad (1)$$

$$\lambda_h = [E_0^+ - E^+] + [E_0^0 - E_0] \quad (2)$$

In the context of electronic energies, E_0^- and E_0^+ represent the anions' and cations' energies, respectively, obtained from their optimized constructions in ground state. On the other hand, E_0^- and E_0^+ correspond to the neutral anions' and cations' energies, respectively. Finally, E_0^0 represents the neutral molecule's energy.

3. Results and Discussion

R has been used as our reference. Five new molecules having the following acceptors (end groups) were created by modifying the R molecule's end group. (1): (Z)-2-(5',6'-dimethoxy-2-methylene-3,3'-dioxo-2,3-dihydro-[1,2'-biindenylidene]-1'(3'H)-ylidene)malononitrile (2): (Z)-2-(5',6'-dimethoxy-2-methylene-3,3'-dioxo-2,3-dihydro-[1,2'-biindenylidene]-1'(3'H)-ylidene)malononitrile, (3) (Z)-2-(6'-fluoro-5'-methoxy-2-methylene-3,3'-dioxo-2,3-dihydro-[1,2'-biindenylidene]-1'(3'H)-ylidene)malononitrile, (4)(Z)-2-(6'-fluoro-5'-methoxy-2-methylene-3,3'-dioxo-2,3-d

ihydro-[1,2'-biindenylidene]-1'(3'H)-ylidene)malononitrile,(5) (Z)-1'-(dicyanomethylene)-2-methylene-3,3'-dioxo-1',2,3,3'-tetrahydro-[1,2'-biindenylidene]-5',6'-dicarbonitrile. Thiazole bridges connect all the aforementioned acceptors to the IDT core. All of these compounds' optoelectronic and photochemical characteristics were investigated using the above-mentioned functional B3LYP via DFT computations at 6-31G (d, p) basis set that had default spin.

3.1. Optimized Geometries

Figure 3 depicts the Reference's ground state geometry alongside engineered components. The IDT core of all molecules is the same, but the acceptor groups are varied. The dihedral angle between acceptor groups and bridges (Φ_a) alongside the core and bridges (Φ_b) (provided in Table 1) is a useful tool for explaining the structure's planarity. The values of (Φ_a) and (Φ_b) for R alongside all the created molecules are acquired through their optimised files and range between 0.003 and 0.53 and 0.12 to 0.94 respectively, emphasizing their planar arrangement. Their planar shape encourages charge transfer between molecules, which increases their photovoltaic features [35, 36].

Table 2 also includes C-C bond length estimates among acceptor units and bridges (La) and bridges together with cores (Lb). These readings fall within an array of 1.41 to 1.44, implying the bond length falls in between single (1.54)

and double (1.34) and looks closer to the double bond. This region suggests an existence of conjugation owing to π -electrons resonating between center and acceptors. The rise in conjugation promotes better charge transmission as well as

the Bathochromic shift that improves the molecule's absorption of radiations. As a result, OSCs with wider absorption range may be produced.

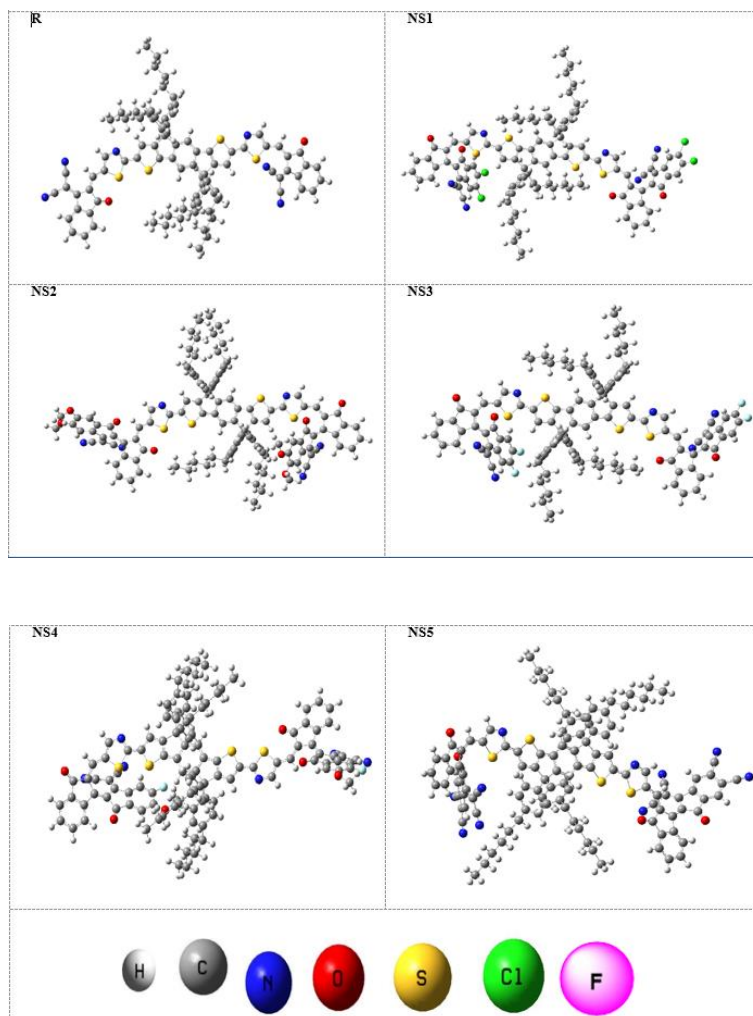


Figure 3. Adjusted geometries of *R* and newly designed molecules.

Table 1. Simulated dihedral angles and bond lengths of *R* and NS1-NS5.

Molecules	Bond length La	Dihedral angle Φ_a	Bond length Lb	Dihedral angle Φ_b
R	1.42	0.0032	1.43	0.52
NS1	1.41	0.37	1.43	0.94
NS2	1.41	0.53	1.43	0.89
NS3	1.42	0.28	1.43	0.12
NS4	1.41	0.013	1.44	0.13
NS5	1.41	0.2	1.43	0.23

3.2. Frontier Molecular Orbital (FMO)

The study of frontier molecular orbitals is crucial for investigating the optical and electrical characteristics of molecules. According to the literature review, any variation in a molecule's photoelectric property is calculated according to the allocation of FMOs, i.e., HOMO and LUMO. According to band theory, a molecule's HOMO is known as conduction band, whereas its LUMO is known as valence band [37-41].

In our research, we observed that E_{HOMO} and E_{LUMO} of all the freshly created molecules (NS1-NS5) were greater compared to those of (R). This boost in energy is potentially due to a larger degree of conjugation within the end portions linked to symmetrical central component. Consequently, there was a corresponding increase in λ_{max} throughout the absorption spectrum. Table 2 depicts the HOMO and LUMO energies, alongside their energy band gaps.

The molecular orbital diagrams of the R and created substances (NS1-NS5) can be seen in Figure 4.

Table 2. HOMO and LUMO energy levels and band gap of R and freshly created molecules.

Molecules	E_{HOMO}	E_{LUMO}	E_g
R	-5.43	-3.40	2.03
NS1	-5.52	-3.73	1.78
NS2	-5.29	-3.39	1.91

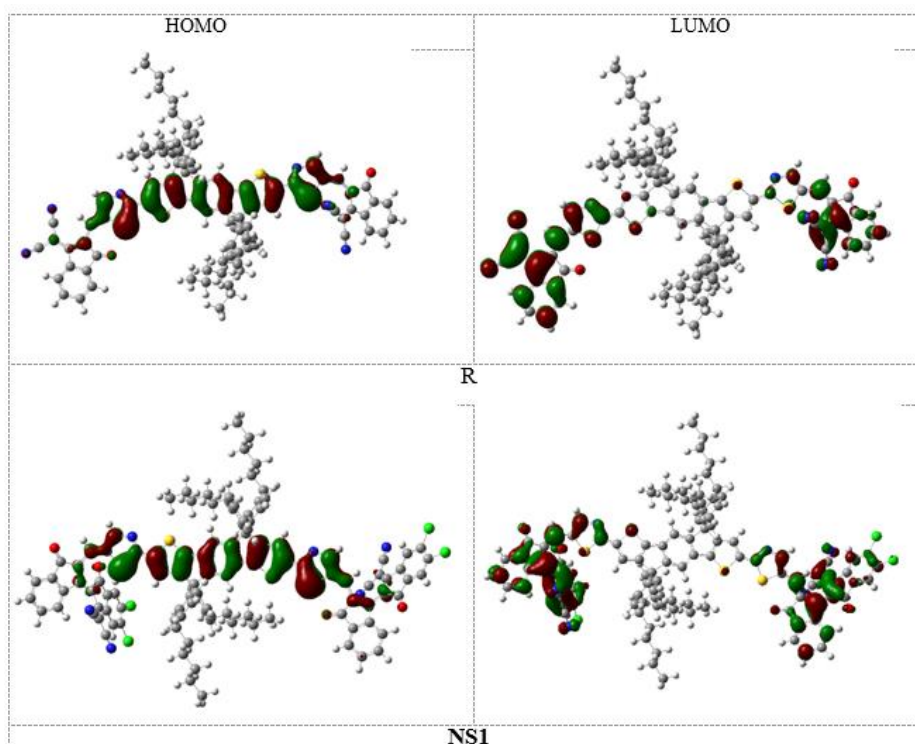
Molecules	E_{HOMO}	E_{LUMO}	E_g
NS3	-5.48	-3.67	1.81
NS4	-5.46	-3.55	1.92
NS5	-5.74	-4.07	1.67

Largely electron density is distributed from core to Thiazole π -linker in ground state and shifted to the end units in excited state, as seen in Figure 4. R's HOMO in excited state possesses energy of 5.43eV, which increases to 3.40eV and energy gap separating these MOs is estimated as 2.03eV. During excitation, electron density migrated from the donor portion to the acceptor portions.

The ground state energies of the rest of the molecules NS1 NS2, NS3, NS4 and NS5 are 5.52 eV, 5.29 eV, 5.48 eV, 5.46eV and 5.74 eV, accordingly, with LUMO energies of 3.73 eV, 3.39 eV, 3.67 eV, 3.55eV and 4.07 eV with band gaps of 1.78 eV, 1.91 eV, 1.81 eV, 1.92eV and 1.67 eV. Following Table 2 exhibits that there is nearly no variation in band energy between NS2 and NS4, whereas NS5 has the lowest band gap. The following pattern was noticed when these molecules were organised in increasing sequence of their energy gap.

$$\text{NS5} < \text{NS1} < \text{NS3} < \text{NS2} < \text{NS4} < \text{R}$$

Figure 5 portrays the HOMO and LUMO energies, along with the energy band gaps of R and freshly created molecules.



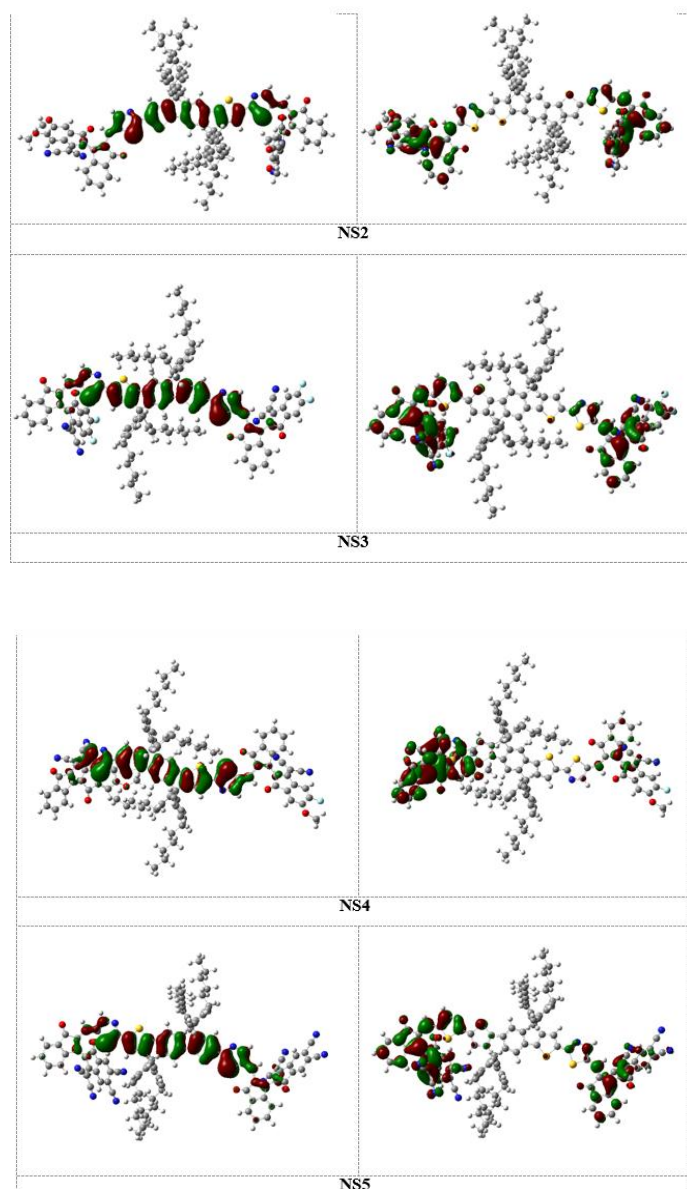


Figure 4. FMO geometries of R as well as freshly created molecules.

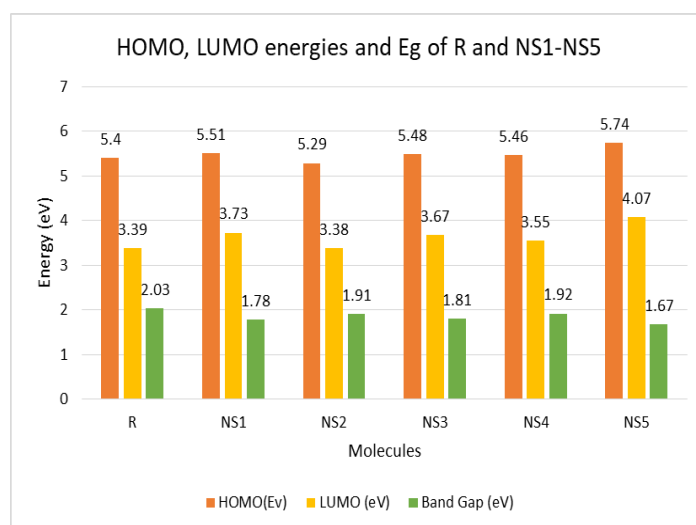


Figure 5. E_g , E_{HOMO} and E_{LUMO} of R and proposed molecules NS1-NS5.

3.3. Partial Density of States (PDOS)

DOS (density of states) study took place at the designated functional for the model and other SM NFAs (Figure 6). DOS describes the electron density transported from core counterpart to acceptor counterpart [42, 43]. R and freshly created molecular configurations were divided in three parts

for DOS analysis: the central core D followed by π -linker L and terminal acceptor portion. The density of states graph depicts the availability of states at different energies within various moieties of new molecular frameworks. The region beneath the graph's curves indicates the accessible regions for charge excitation.

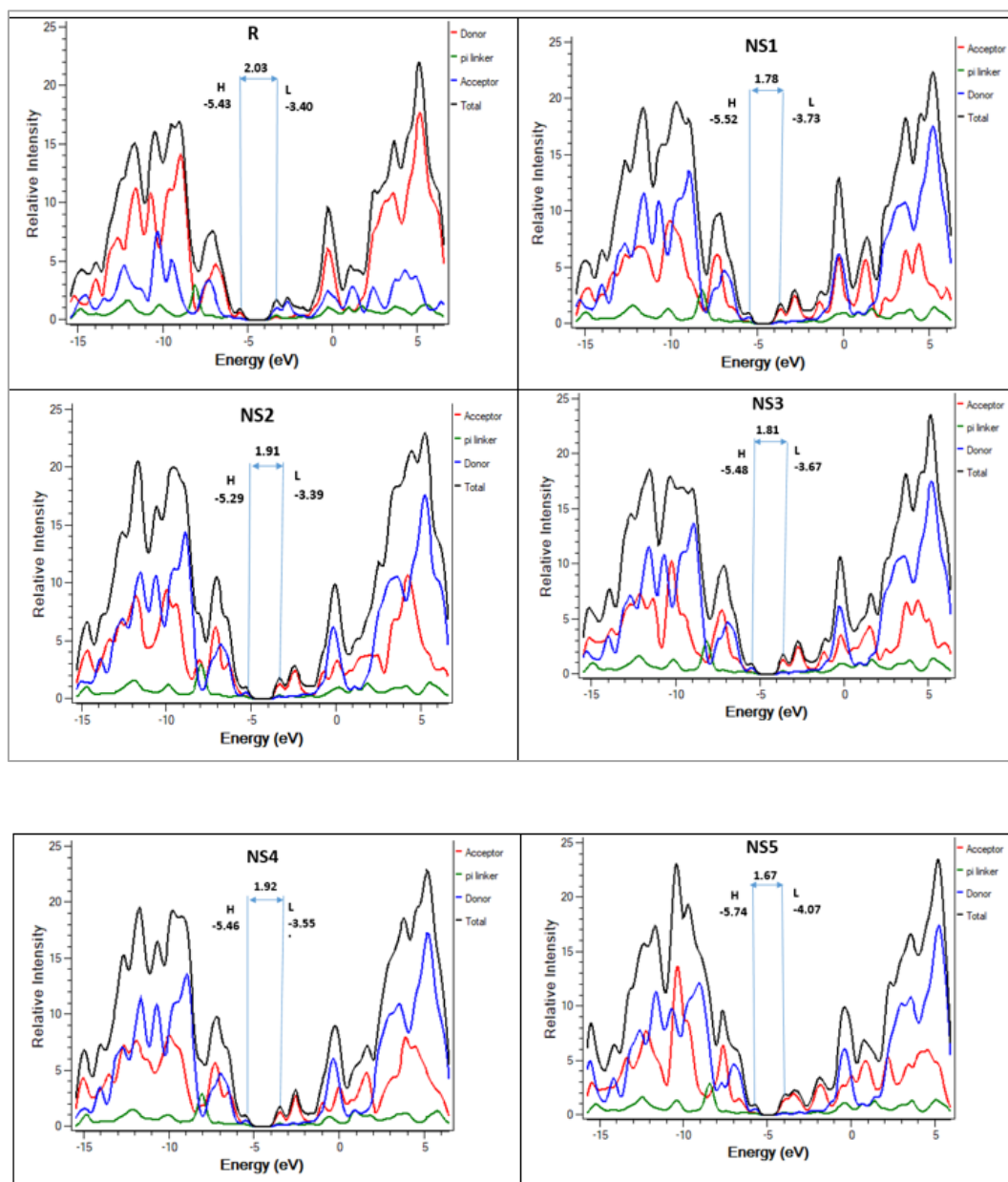


Figure 6. PDOS graphs of R and NS1-NS5.

For the examination of each fragment's participation in the overall absorption region and its electronic dispersion, DOS of chosen moieties NS1-NS5 was computed at B3LYP/6-31G level followed by comparison with R. The left section of the PDOS graphic picture displays the HOMO zone, while the right section indicates LUMO zone of R and

novel created molecules. As illustrated in Figure 6, each selected molecule is separated into three pieces: the centre portion, Thiazole Bridge and acceptor. The core unit played an important part in the overall population, as seen by the contribution they made to each molecule. Thiazole Bridge connects these core components to acceptor sections. Thiazole

Bridge as well contributes to electron delocalization due to the participation of π -conjugation, as seen in the diagrams for each molecule.

The contribution of the centre (55.4%) is greater compared to the portion of the acceptor (20%) in the formation of R's HOMO, showing that electrons' placement of HOMO is extra focused on donor. The contribution of the center (15.2%) to the development of R's LUMO is smaller as opposed to contribution of acceptor (65.4%), showing that the LUMO is more focused on the acceptor component. In a similar way the cores of NS1-NS5 contribute 61.5, 59.9, 61.5, 60.3 and 61.6% to the production of their HOMO, accordingly. This suggests that the contribution of centres of NS1-NS5 in HOMO generation is greater as compared to the centre of R (55.4%). However, the HOMOs of all proposed molecules are more focused on their cores than on their acceptors (the

percentage contributions of R and NS1 to NS5 acceptors in HOMO development are 20%, 19.8%, 20.6%, 19.6%, 19.8% and 20.4%, respectively). Bridges' percentage contribution to R HOMO output and the values for NS1-NS5 are 24.6, 18.7, 19.4, 18.9, 19.9 and 18.0%, correspondingly.

Likewise, the LUMO of crafted molecules is primarily focused on acceptors (the percentage contributions of acceptor sections in NS1-NS5 are 69.6, 66.7, 69.1, 69.1 and 71.7%, in that order) than on centres (the percentage contributions of centres in NS1-NS5 are 12.8, 14.5, 13.1, 13.5 and 12.2%, accordingly) as seen in the [table 3](#). The percentage contribution of developed compounds' acceptors to LUMO generation is bigger than that of R (65.4%). Bridges provide 19.4, 7.6, 18.8, 17.8, 17.4 and 17.2% of LUMO production in R and NS1-NS5, respectively.

Table 3. % contribution of Centre and Acceptors towards HOMO and LUMO of R and newly constructed molecules.

molecules	MOs	% contribution of acceptor	% contribution of pi linker	% contribution of donor
R	HOMO	20.0	24.6	55.4
	LUMO	65.4	19.4	15.2
NS1	HOMO	19.8	18.7	61.5
	LUMO	69.6	17.6	12.8
NS2	HOMO	20.6	19.4	59.9
	LUMO	66.7	18.8	14.5
NS3	HOMO	19.6	18.9	61.5
	LUMO	69.1	17.8	13.1
NS4	HOMO	19.8	19.9	60.3
	LUMO	69.1	17.4	13.5
NS5	HOMO	20.4	18.0	61.6
	LUMO	70.7	17.2	12.2

By carefully analysing these outcomes, we are able to determine that a superior charge transfer took place from center to the acceptor in newly established molecules NS1-NS5 than in R since the percentage contribution made by the centre in HOMO construction is lower than R and its acceptor's contribution in LUMO construction is larger than R, presumably due to greater electron withdrawing skills of established compounds' acceptors. Pi-linkers also facilitated charge transfer across core towards acceptors by providing extended pi conjugation. These outcomes are also shown graphically in [Figure 6](#), where HOMO/LUMO energies and associated E_{gap} are shown which clearly matched the HOMO/LUMO energies and E_{g} calculated by FMO.

The preceding discussion indicated that there is strong consistency between the FMO and DOS computations, with both highlighting that the HOMO energy levels have a greater focus on the core, whereas the LUMO energy levels are more focused upon the acceptor groups and that an effective transfer of charges has occurred between the centre and acceptors of the established molecules, making them excellent options for the manufacturing of productive OSCs.

The optimal electron density transitioning to R and freshly created compounds decreases in the subsequent sequence.

$$\text{NS5} > \text{NS1} > \text{NS3} > \text{NS4} > \text{NS2} > \text{R}$$

3.4. Molecular Electrostatic Potential (MEP)

The MEP is essential for comprehending the charge distributions and charge-related characteristics of molecules through its three-dimensional diagrams. These diagrams provide a visual representation of the MEP and are useful in various applications such as identifying reactive sites for electrophilic and nucleophilic attacks and investigating hydrogen bonding interactions [44, 45]. The MEP is significant because it combines information about the molecular size, shape and electrostatic potential, including positive, negative and neutral regions, which are depicted using color grading. Each color corresponds to a specific value of the electrostatic potential at the surface, with red indicating regions of the most negative electrostatic potential. Blue is used to represent regions with the highest positive electrostatic potential [46].

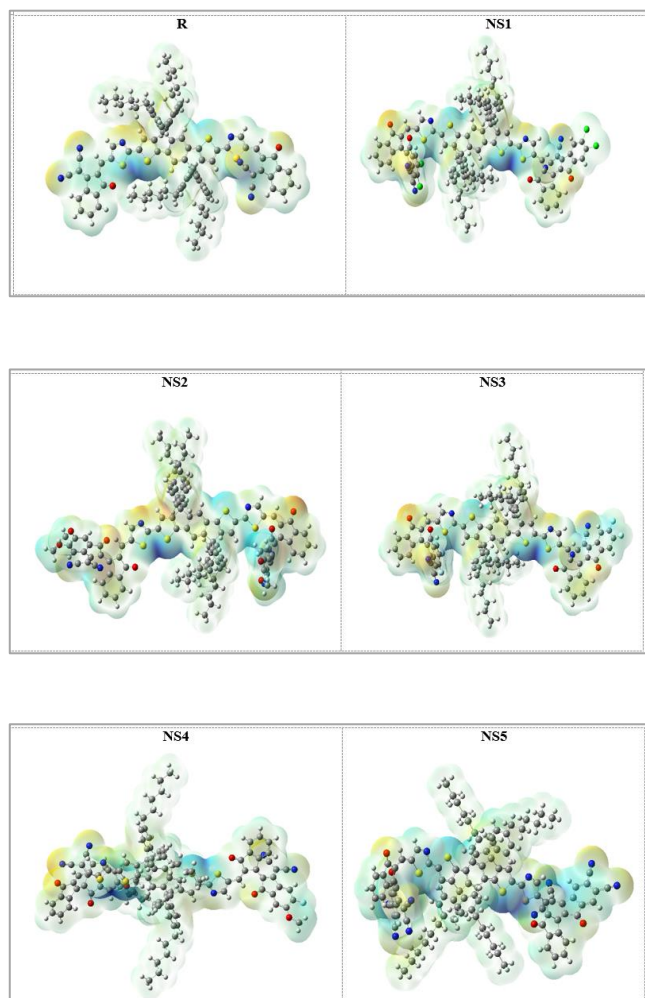


Figure 7. Visual representation of MEP structures of R and newly created molecules.

In particular, the electron-accepting units located on the acceptor side of the reference molecule R and the freshly designed compounds (NS1-NS5) are represented in red, indicating electron deficiency. On the other hand, the donor

parts of the molecules are shown in blue, indicating electron richness as shown in Figure 7. The modification in end units provides the electron-withdrawing ability to the acceptor portion of the OSCs, which facilitates productive operation and electron transfer processes. The presence of electron-deficient regions in the molecules enhances their ability to capture and transport electrons, contributing to the overall performance of the PSCs.

3.5. Optical Properties

The TD-DFT method was implemented to study the absorption spectrum of all the investigated moieties in both the chloroform and gaseous phase. The IEFPCM model utilized for solvation in the current study was projected in the chloroform solvent.

According to preceding considerations, all engineered molecules exhibit efficient absorption properties in the visible part of the absorption spectrum.

We juxtaposed the absorption of designed moieties in the gas phase to that of chloroform in the liquid phase to investigate the impact of the solvent on the absorption coefficient. In an atmosphere of chloroform solvent, the absorption band migrated towards the redshift, indicating that the solvent had a substantial part in expanding the absorption range. Because of the stabilization of delocalized π -electrons in the presence of a solvent such as chloroform, the band of absorption shifted to a longer wavelength. These molecules, on the contrary, have lesser absorption in the gas phase. NS1, NS2, NS3, NS4 and NS5 absorbance values determined at the B3LYP/6-31G level of DFT with the presence of chloroform solvent were 867 nm, 805 nm, 848 nm, 828 nm and 921 nm, accordingly (Table 4). The Maximum absorption bands were detected in the gaseous phase at 691 nm, 817 nm, 764 nm, 802 nm and 870nm for NS1, NS2, NS3, NS4 and NS5 in that order (Table 5).

The maximum value is listed in the following sequence for both the solvent and gaseous phases accordingly:

$$\text{NS5} > \text{NS1} > \text{NS3} > \text{NS4} > \text{NS2} > \text{R}$$

$$870 > 867 > 848 > 828 > 805 > 733$$

$$870 > 817 > 802 > 768 > 764 > 691$$

The lowest amount of energy necessary to excite electrons through ground to the excited state is termed as the excitation energy. It is often referred to as the optical band gap. Ex in the solvent phase for the examined compounds is less than that in the gas phase, indicating that these molecules have superior charge transfer capacity in the solvent phase than in the gas phase. Newly tailored molecules exhibited lower excitation energy than R, with NS5 having the lowest excitation energy of 1.42eV. All of the new compounds possessed lower excitation energies than R, implying that this makes them far more effective. As an outcome, we are able to illustrate that each one of the developed molecules is suitable for PSCs with

higher productivity.

Table 4. Computationally calculated optical properties of R and engineered molecules in chloroform solvent.

Molecule	Determined λ_{max}	Experimental λ_{max}	Translational Energy	Osc. Strength	Assignment
R	733	666	1.69	2.3181	HOMO->LUMO (98%)
NS1	867		1.43	1.8435	HOMO->LUMO (96%)
NS2	805		1.54	1.992	HOMO->LUMO (95%)
NS3	848		1.46	1.8472	HOMO->LUMO (96%)
NS4	828		1.50	1.418	HOMO->LUMO (95%)
NS5	921		1.42	1.5407	HOMO->LUMO (97%)

Table 5. Computationally calculated optical properties of R and engineered molecules in gaseous phase.

Molecule	Determined λ_{max}	Experimental λ_{max}	Translational Energy	Osc. Strength	Assignment
R	691	666	1.72	2.1345	HOMO->LUMO (97%)
NS1	817		1.52	1.6313	HOMO->LUMO (97%)
NS2	764		1.62	1.7664	HOMO->LUMO (96%)
NS3	802		1.54	1.6244	HOMO->LUMO (97%)
NS4	768		1.61	1.3211	HOMO->LUMO (95%)
NS5	870		1.43	1.4378	HOMO->LUMO (95%)

Oscillator strength (f) serves as a dimensionless number that indicates radiation emission or absorption caused by electron excitation between two energy levels. The power of the oscillator for organic chromophores is increased, resulting in high absorption in the UV-Visible range. R and designated molecules have comparable oscillator strengths due to presence of thiazole bridges.

3.6. Dipole Moment

The dipole moment constitutes a polarity measuring method used to determine if the studied system is capable of arranging stable molecule packing that results in high crystallinity. The higher the degree of polarity of the molecule, the more stable the crystalline packing. Any molecular framework with a solid crystal structure can minimize abnormalities in donor and acceptor surface contact.

Less anomalous conditions increase the likelihood of charge production at the interface. NS2, NS4 and NS5 exhibit the higher dipole moments than R. Therefore, modifying the terminal unit is an effective method to achieve highly functional PSC with enhanced capabilities. Dipole moments of R and engineered moieties in gaseous as well as solvent phase

are displayed in Table 6.

Table 6. Dipole moments of R and engineered molecules in gaseous and solvent phase.

Molecule	Dipole moment in gaseous phase	Dipole moment in solvent phase
R	6.3390	8.3520
NS1	3.7695	4.1368
NS2	10.8401	13.5010
NS3	3.0395	3.1432
NS4	10.6139	13.2386
NS5	12.0299	12.1546

3.7. Light-Harvesting Efficiency (LHE)

Light harvesting efficiency refers to the material's ability to collect light for charge creation or charge generation into the conduction band. It is also an essential concern for materials

utilized in solar cells. According to the equation below, LHE maintains a direct relationship with J_{sc} :

$$J_{sc} = \int_{\lambda}^0 LHE(\lambda) \cdot \Phi_{inj} \cdot \eta_{collect} \cdot d\lambda \quad (3)$$

Where LHE stands for light-harvesting efficiency, Φ_{inj} stands for electron injection and $\eta_{collect}$ is for nearly constant charge collection. Since the above equation connects LHE to short circuit current, it has been calculated and felt that variations in LHE have an immediate impact on J_{sc} . The equation [4] was used to determine LHE.

$$LHE = 1 - 1^{-f} \quad (4)$$

Where f denotes oscillator strength. The greatest oscillator strength was used for LHE ascription, resulting in a λ_{max} of UV-Vis spectra simulated utilizing the TD-DFT B3LYP/6-31G (d,p) technique. This means that the LHE calculated is the greatest efficiency with which a PSC active material can capture light. Furthermore, R and NS2 have a greater LHE and a greater short circuit current and are regarded as advantageous molecules for solar cells (Table 7).

Table 7. LHE and Oscillator strength of R and newly developed molecules.

Molecule	Oscillator strength	LHE
R	2.3181	0.9952
NS1	1.8435	0.9857
NS2	1.9920	0.9898
NS3	1.8472	0.9858
NS4	1.4180	0.9616
NS5	1.5407	0.9712

3.8. Transition Density Matrix (TDM) and Binding Energies (Eb)

TDM at the excited state might estimate the characteristics of an electronic transition for small molecules. The interaction that occurs within acceptor and donor components in the first excited state, electron excitation and exciton localization or delocalization are key elements of the TDM technique. Atoms of Hydrogen were excluded by convention when generating the TDM graphs owing to their small influence on these charts. Its two significant properties, charge transfer state (off-diagonal configuration) with locally excited state (diagonal configuration), give valuable insights about the pattern of electron-hole kinetics and their electron density in a particular region of the electron density spectrum. The 2D charts of TDM generated by using Multiwfn software offer a graphical representation for the examination of electron primary sites.

TDM molecules were divided into three groups for analysis: the central core (D), the π -linker (L) and the acceptor group (A). The x-axis at the bottom and the y-axis on the left of the TDM plots of the molecules (Figure 8) show the total number of atoms, whereas the y-axis on the right hand reflects the charge density, which rises from bottom (dark blue) until the top (brighter section).

TDM map investigation describes electron transport from donor towards acceptor components in the excited state. When we work our way up from the bottom of the figure, density of electrons shifts diagonally from the central donor to the acceptor area, where nucleophilicity is greatest. It demonstrates that all engineered molecules (NS1-NS5) and R are extremely effective because the electron moves in the correct direction, i.e., towards the acceptor area. However, when matching R to the tailored molecules, the engineered moieties had more nucleophilicity towards the acceptor area than R. NS5 and NS2 are the best choices among the five customized molecules, with the largest electronic abundance in the acceptor portion. Another one, NS4, displays a higher shift of the electron density towards the acceptor portion, with the majority of the electron concentration lying in the acceptor portion. This progress in our proposed molecules is because of the modifications in acceptor regions that is the displacement of the electron withdrawing groups in acceptor region, as previously mentioned.

The exciton binding energy (Eb) is another relevant characteristic for evaluating the optoelectronic features of OSCs. This exciton binding energy characterizes the separation potential of exciton and it is related to the Coulombic force of attraction amid hole and electron. Eb and the columbic force of attraction have a direct link. Exciton dissociation is inversely related to attraction forces, implying that less columbic interaction leads in less binding energy and a larger dissociation potential of exciton in excited state. The following equation is a theoretical technique to estimate the exciton binding energy.

$$E_b = E_g - E_x \quad (5)$$

Where E_g and E_x indicate, respectively, the initial excitation energy and the band gap. Table 8 lists the exciton binding energy as a reference and the compounds examined. The greater exciton dissociation is specified by the least exciton binding energy for NS5. As a result, NS5 has more charge mobility than other created molecules.

Table 8. Simulated energy gap, E_x and E_b values.

Molecule	E_g (eV)	E_x (eV)	E_b (eV)
R	2.03	1.69	0.34
NS1	1.78	1.43	0.35

Molecule	E_g (eV)	E_x (eV)	E_b (eV)
NS2	1.91	1.54	0.37
NS3	1.81	1.46	0.35
NS4	1.92	1.50	0.42

Molecule	E_g (eV)	E_x (eV)	E_b (eV)
NS5	1.67	1.42	0.25

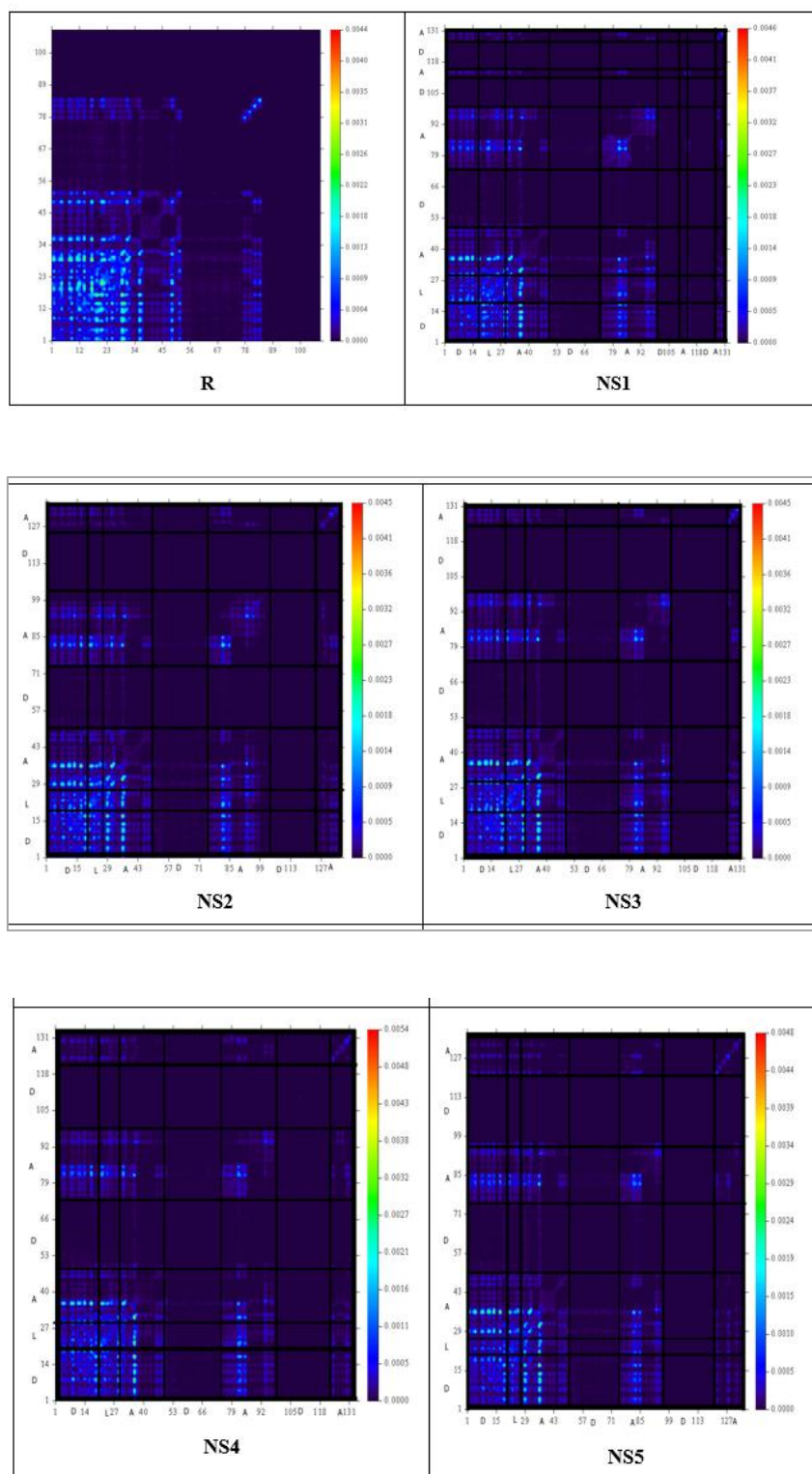


Figure 8. TDM maps of reference and newly created molecules (NS1-NS5).

3.9. Charge Mobility and Charge Transfer Integral

Charge transfer integral is an important aspect in defining charge transport parameters.

The transfer integral is very sensitive to the relative location of interacting molecules in the crystal as well as the packing patterns and is dependent on the interaction involving neighbouring molecules. Because of strong intermolecular contacts, π -stacking and face-to-edge stacking have better charge transmission. Eq (6) and Eq (7) represent charge transfer integral of hole and electron accordingly.

$$t_{hole} = \frac{1}{2}(E_H - E_{H-1}) \quad (6)$$

$$t_{electron} = \frac{1}{2}(E_{L+1} - E_L) \quad (7)$$

The charge mobility rates can help us analyse the efficiency with which charge is carried in our OSC systems. Because of

its dependency on reorganisation energy (the lower the amount of reorganisation energy, the greater the mobility of charges), charge transfer mobility may be effortlessly explored. The energy of reorganisation consists of 2 major components: internal and external energy of reorganisation. Our major focus here is on the interior one, while the exterior outcomes are omitted since they deal with external conditions that are impossible to assess using our computational approaches.

Eq. (1) was used to investigate the internal energies of reorganisation for electrons (e). The results shown in Table 9 demonstrated the sequence of reorganisation energies in R and designed compounds. Table 10 exhibits that the electron mobilities of R, NS1, NS2, NS3 and NS4 are comparable, while NS5 shows highest charge mobilities emphasizing its superior operation in OSCs. Examining the energy of reorganisation, it may be determined that NS5 will perform more effectively after implanted in OSCs.

Table 9. E_H , E_L , E_{H-1} , E_{L+1} and charge mobilities of R and newly engineered molecules.

Molecule	E_H	E_L	E_{H-1}	E_{L+1}	t_{hole}	$t_{electron}$
R	-5.43	-3.40	-6.07	-3.21	0.32	0.09
NS1	-5.52	-3.73	-6.06	-3.74	0.27	0.005
NS2	-5.29	-3.39	-5.79	-3.24	0.25	0.075
NS3	-5.48	-3.67	-6.03	-3.54	0.28	0.065
NS4	-5.46	-3.55	-5.98	-3.40	0.25	0.075
NS5	-5.74	-4.07	-6.30	-3.92	0.28	0.075

The frequently cited charge transfer rates from classical Marcus theory is as follows:

$$k_{ct} = \frac{4\pi^2}{h} \frac{V^2}{\sqrt{4\pi\lambda k_B T}} \exp\left\{-\frac{\lambda}{4k_B T}\right\} \quad (8)$$

Here λ is the charge transport reorganisation energy, V is the transfer integral of nearby molecules, k_B and T are Boltzmann constant and temperature and h is the Plank con-

stant. The reorganisation energy and charge transfer integral clearly dominate the transfer rate.

Small internal reorganisation energy and large intermolecular transfer integrals, based on the Marcus formula, serve to accelerate charge transfer processes between neighbouring molecules. Furthermore, we also determined the E_{H-1} (one orbital below HOMO) and E_{L+1} (one orbital above LUMO) as evident by Table 9.

Table 10. Electron and hole mobilities of R and newly engineered compounds.

Molecule	λ_e	λ_h
R	0.0062	0.0062
NS1	0.0069	0.0067
NS2	0.0085	0.0073

Molecule	λ_e	λ_h
NS3	0.0071	0.0067
NS4	0.0082	0.0143
NS5	0.0057	0.0069

3.10. Open Circuit Voltage (V_{oc}), Normalized V_{oc} and Fill Factor

V_{oc} is a favourable measure that reflects the efficacy of solar devices. It depicts the maximum quantity of current that may be generated by electrical devices with zero-voltage supply. V_{oc} is primarily linked with the HOMO and LUMO groups of donors and acceptors. V_{oc} is primarily influenced by parameters such as light intensity, e-h recombination capacity, temperature and system's shape. The V_{oc} is calculated using the following equation:

$$V_{oc} = \frac{ELUMO \text{ OF ACCEPTOR} - EHOMO \text{ OF DONOR} - 0.3}{e} \quad (9)$$

Here 0.3 represents the voltage loss and e represents the elementary charge on a single molecule (considered as 1). PTB7-Th's HOMO and LUMO energies are 5.20 and 3.60 eV,

correspondingly. V_{oc} of the R and customized compounds is computed. Because the compounds under investigation function as acceptors, PTB7-Th is designated as the donor component. The theoretical values for R, NS1, NS2, NS3, NS4 and NS5 are 1.5 V, 1.17 V, 1.51 V, 1.23 V, 1.35 V and 0.83 V respectively. Figure 9 depicts the V_{oc} curve of R and corresponding acceptor choices (NS1-NS5) linked with donor PTB7-Th.

The results of Eq. (9) are summarised in Table 11, indicating that R and NS2 have a more substantial V_{oc} (due to thiazole-bridges and methoxy based acceptor sections at terminal parts) whereas NS1, NS3, NS4 and NS5 likewise possess good V_{oc} values, they demonstrated a reduced gap in both the Donor's HOMO and Acceptor's LUMO that might lead to a slight decline in their V_{oc} . However, in the long term, their reduced gap will enhance the value of shortcircuit current density (J_{sc}), which is also significant in improving PCEs.

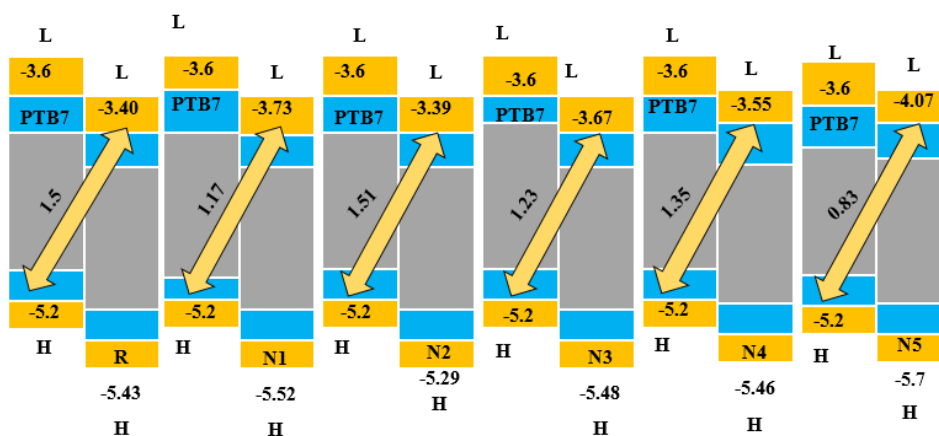


Figure 9. Simulated V_{oc} values of R and newly engineered compounds.

Table 11. V_{oc} , normalized V_{oc} and fill factor of R and newly engineered compounds.

Molecules	V_{oc}	Normalized V_{oc}	Fill Factor
R	1.50	58.07	0.9142
NS1	1.17	44.30	0.8874
NS2	1.51	58.46	0.9156
NS3	1.23	47.62	0.8996

Molecules	Voc	Normalized Voc	Fill Factor
NS4	1.35	52.26	0.9067
NS5	0.83	32.13	0.8645

The optoelectronic yield of any system may be calculated using the fill factor, which is derived by the equation below.

$$FF = \left[\frac{\left(\frac{eV_{oc}}{k_b T} - \ln \left(\frac{eV_{oc}}{k_b T} + 0.72 \right) \right)}{\frac{eV_{oc}}{k_b T} + 1} \right] \quad (10)$$

Where 'Kb' symbolises Boltzman's constant, 'T' symbolises temperature (300 K) and 'e' symbolises the elementary charge with a value of 1. The total quantity (eVoc/KbT) corresponds to the normalised Voc. In comparison to R, NS2 had higher FF values demonstrating the capacity of the developed chemicals to act well in OSCs. Furthermore, the rest of the constructed molecules had comparable FF values.

Based on the preceding explanation, a decent estimate of the PCEs of developed molecules can be done by focusing on Eq. (11).

$$PCE = \left(\frac{FF \times Voc \times J_{sc}}{P_{input}} \right) \quad (11)$$

P_{input} denotes the power related to light that enters. J_{sc} is affected by several elements including band gap, LHE, charge mobility rate and so on. All of them are computed in this work, which highlights the greater J_{sc} values of designed compounds than R. likewise, they have comparable FF and Voc values, which hinted at their improved application in OSCs. NS2 demonstrated an improvement in Voc and FF versus R, proving its capacity to increase the PCEs of PVs.

4. Conclusion

We have developed five innovative acceptor entities based on SMA design, where the acceptor components N1-N5 were incorporated with an IDT core component. The configuration, photosensitivity and photochemical properties of these newly designed components are being calculated using quantum chemistry methods. Based on FMO studies, all the newly designed NFAs exhibited lower energy levels in their MOs compared to the reference molecule (R). This resulted in smaller band gaps and transition energies for the NFAs, with NS5 showing the lowest band gap and transition energy values. Optical analyses conducted in chloroform solution indicated that the newly created particles exhibited a red shift in their absorption spectra compared to R, with higher maximum absorption values. Among the NFAs, NS5 exhibited the highest λ_{max} . Additionally, the reorganization energy and

charge mobility were investigated. NS5 showed the lowest reorganization energies, indicating favorable charge transfer and higher charge mobilities. The other components showed comparable values for reorganization energy. These experimental results highlight that the newly created NFAs, particularly NS5, are well-suited for utilization in OSCs to enhance their optoelectronic and photochemical properties.

5. Future Directions

This investigation offers valuable insights for synthetic chemists seeking to develop high-performance OSCs. Furthermore, computational chemistry approaches, such as scaling methods can be employed to optimize photovoltaic properties. Future research directions may involve further tailoring the acceptor and donor components to enhance overall efficiency.

Abbreviations

NFAs	Non-Fullerene Acceptors
PSCs	Polymer Solar Cells
R	Reference
OSCs	Organic Solar Cells
B3LYP	Becke 3 Term, Lee Yang, Parr
ICT	Intra-molecular Charge Transfer
E_g	Energy Gap
PCE	Power Conversion Efficiency
PDOS	Partial Density of States
CPCM	Conductor Like Polarizable Continuum Model
BHJ	Bulk Hetero Junction
FF	Fill Factor
V_{oc}	Open Circuit Voltage
J_{sc}	Short Circuit Current
DFT	Density Functional Theory
HOMO	Highest Occupied Molecular Orbital
LUMO	Lowest Unoccupied Molecular Orbital
F	Oscillator Strength
λ_e	Electron Reorganization Energy
λ_h	Hole Reorganization Energy
TDM	Transition Density Matrix
UV	Ultra Violet
E_b	Exciton Binding Energy
CT	Charge Transfer
FMO	Frontier Molecular Orbital

Author Contributions

Neelam Shahzadi: Conceptualization, Investigation, Methodology, Visualization, Writing – original draft, Writing – review & editing

Iqra Naz: Data curation, Formal Analysis, Funding acquisition, Resources

Rehmat Illahi: Project administration, Software, Supervision, Validation

Conflicts of Interest

The authors declare no conflicts of interest.

References

- [1] AV Rodrigues, DAR de Souza, FDR Garcia, Sidney, Renewable energy for a green future: Electricity produced from efficient luminescent solar concentrators. 2022. <https://doi.org/10.1016/j.seja.2022.100013>
- [2] Farhat, A., et al., Tuning the optoelectronic properties of Subphthalocyanine (SubP1). Farhat, A., et al., Tuning the optoelectronic properties of Subphthalocyanine (SubPc) derivatives for photovoltaic applications. 2020. 107: p. 110154. <https://doi.org/10.1016/j.optmat.2020.1101>
- [3] Nelson, D. L., A. L. Lehninger and M. M. Cox, Lehninger principles of biochemistry. 2008: Macmillan. <https://doi.org/10.1007/978-3-662-08289-8>
- [4] Askari Mohammad Bagher, Mirzaei Mahmoud Abadi Vahid, Mirhabibi Mohsen. Types of Solar Cells and Application. American Journal of Optics and Photonics. Vol. 3, No. 5, 2015, pp. 94-113. <https://doi.org/10.11648/j.ajop.20150305.17>
- [5] Yao, H., et al., Molecular design of benzodithiophene-based organic photovoltaic materials. 2016. 116(12): p. 7397-7457. <https://doi.org/10.1021/acs.chemrev.6b00176>
- [6] Lin, Y. and X. J. A. o. c. r. Zhan, Oligomer molecules for efficient organic photovoltaics. 2016. 49(2): p. 175-183. <https://doi.org/10.1021/acs.accounts.5b00363>
- [7] Lin, Y., Y. Li and X. J. C. S. R. Zhan, Small molecule semiconductors for high-efficiency organic photovoltaics. 2012. 41(11): p. 4245-4272. <https://doi.org/10.1039/c2cs15313k>
- [8] He, Y. and Y. J. P. c. c. p. Li, Fullerene derivative acceptors for high performance polymer solar cells. 2011. 13(6): p. 1970-1983. <https://doi.org/10.1039/C0CP01178A>
- [9] Li, C.-Z., H.-L. Yip and A. K.-Y. J. J. o. M. C. Jen, Functional fullerenes for organic photovoltaics. 2012. 22(10): p. 4161-4177. <https://doi.org/10.1039/C2JM15126J>
- [10] He, D., et al., A highly efficient fullerene acceptor for polymer solar cells. 2014. 16(16): p. 7205-7208. <https://doi.org/10.1039/C4CP00268G>
- [11] Nielsen, C. B., et al., Non-fullerene electron acceptors for use in organic solar cells. 2015. 48(11): p. 2803-2812. <https://doi.org/10.1021/acs.accounts.5b00199>
- [12] Li, H., et al., Beyond fullerenes: design of nonfullerene acceptors for efficient organic photovoltaics. 2014. 136(41): p. 14589-14597. <https://doi.org/10.1021/ja508472j>
- [13] Chochos, C. L., N. Tagmatarchis and V. G. J. R. A. Gregoriou, Rational design on n-type organic materials for high performance organic photovoltaics. 2013. 3(20): p. 7160-7181. <https://doi.org/10.1039/C3RA22926B>
- [14] Chen, W. and Q. J. J. o. M. C. C. Zhang, Recent progress in non-fullerene small molecule acceptors in organic solar cells (OSCs). 2017. 5(6): p. 1275-1302. <https://doi.org/10.1039/C6TC05066B>
- [15] Bin, H., et al., 11.4% Efficiency non-fullerene polymer solar cells with trialkylsilyl substituted 2D-conjugated polymer as donor. 2016. 7(1): p. 13651. <https://doi.org/10.1038/ncomms13651>
- [16] Zhao, F., et al., Single - junction binary - blend nonfullerene polymer solar cells with 12.1% efficiency. 2017. 29(18): p. 1700144. <https://doi.org/10.1002/adma.201700144>
- [17] Kanwal, N., et al., DFT based modeling of asymmetric non-fullerene acceptors for high-performance organic solar cell. 2022. 54(9): p. 546. <https://doi.org/10.1007/s11082-022-03932-0>
- [18] Scharber, M. C. and N. S. J. P. i. p. s. Sariciftci, Efficiency of bulk-heterojunction organic solar cells. 2013. 38(12): p. 1929-1940. <https://doi.org/10.1016/j.progpolymsci.2013.05.001>
- [19] Chan, S.-H., et al., Synthesis, characterization and photovoltaic properties of novel semiconducting polymers with thiophene– phenylene– thiophene (TPT) as Coplanar Units. 2008. 41(15): p. 5519-5526. <https://doi.org/10.1021/ma800494k>
- [20] Chen, C.-P., et al., Low-bandgap poly (thiophene-phenylene-thiophene) derivatives with broaden absorption spectra for use in high-performance bulk-heterojunction polymer solar cells. 2008. 130(38): p. 12828-12833. <https://doi.org/10.1021/ja801877k>
- [21] Bürkstümmer, H., et al., Tailored merocyanine dyes for solution-processed BHJ solar cells. 2010. 20(2): p. 240-243. <https://doi.org/10.1039/B916181C>
- [22] Mahmood, A., et al., A novel thiazole based acceptor for fullerene-free organic solar cells. 2018. 149: p. 470-474. <https://doi.org/10.1016/j.dyepig.2017.10.037>
- [23] Caricato, M., et al., Gaussian 09: IOps Reference. 2009: Gaussian.
- [24] Dennington, R., T. A. Keith and J. M. J. S. I. S. M. Millam, KS, USA, GaussView 6.0. 16. 2016.
- [25] Bjorgaard, J. A., K. A. Velizhanin and S. J. T. J. o. c. p. Tretiak, Solvent effects in time-dependent self-consistent field methods. II. Variational formulations and analytical gradients. 2015. 143(5): p. 054305. <https://doi.org/10.1063/1.4927167>

- [26] Finley, J. P. J. M. P., Using the local density approximation and the LYP, BLYP and B3LYP functionals within reference-state one-particle density-matrix theory. 2004. 102(7): p. 627-639. <https://doi.org/10.1080/00268970410001687452>
- [27] Yanai, T., D. P. Tew and N. C. J. C. p. I. Handy, A new hybrid exchange–correlation functional using the Coulomb-attenuating method (CAM-B3LYP). 2004. 393(1-3): p. 51-57. <https://doi.org/10.1016/j.cplett.2004.06.011>
- [28] Adamo, C. and V. J. T. J. o. c. p. Barone, Exchange functionals with improved long-range behavior and adiabatic connection methods without adjustable parameters: The m PW and m PW1PW models. 1998. 108(2): p. 664-675. <https://doi.org/10.1063/1.475428>
- [29] Chai, J.-D. and M. J. P. C. C. P. Head-Gordon, Long-range corrected hybrid density functionals with damped atom–atom dispersion corrections. 2008. 10(44): p. 6615-6620. <https://doi.org/10.1039/B810189B>
- [30] Klamt, A., et al., A comprehensive comparison of the IEFPCM and SS (V) PE continuum solvation methods with the COSMO approach. 2015. 11(9): p. 4220-4225. <https://doi.org/10.1021/acs.jctc.5b00601>
- [31] Deschenes, L. A. and A. David A. Vanden Bout University of Texas, Origin 6.0: Scientific Data Analysis and Graphing Software Origin Lab Corporation (formerly Microcal Software, Inc.). Web site: www.originlab.com. Commercial price: 595. Academic price: 446. 2000, ACS Publications.
- [32] JianHua, Z. J. C. and A. Chemistry, Two dimensional graphs of the wave functions in Origin 6.0. 2003. 20(4): p. 467-470.
- [33] Tenderholt, A., PyMOLyze, Version 1.1, in Stanford University. 2006, CA Stanford.
- [34] Marcus, R. A. J. R. o. m. p., Electron transfer reactions in chemistry. Theory and experiment. 1993. 65(3): p. 599. <https://doi.org/10.1103/RevModPhys.65.599>
- [35] Carlotti, B., et al., Charge transfer and aggregation effects on the performance of planar vs twisted nonfullerene acceptor isomers for organic solar cells. 2018. 30(13): p. 4263-4276. <https://doi.org/10.1021/acs.chemmater.8b01047>
- [36] Wang, L., et al., Design and synthesis of dopant-free organic hole-transport materials for perovskite solar cells. 2018. 54(69): p. 9571-9574. <https://doi.org/10.1039/C8CC04026E>
- [37] Khan, M. U., et al., First theoretical framework of triphenylamine–dicyanovinylene-based nonlinear optical dyes: structural modification of π -linkers. 2018. 122(7): p. 4009-4018. <http://dx.doi.org/10.1098/rsos.210570>
- [38] Janjua, M. R. S. A., et al., Effect of π -conjugation spacer (CC) on the first hyperpolarizabilities of polymeric chain containing polyoxometalate cluster as a side-chain pendant: A DFT study. 2012. 994: p. <http://dx.doi.org/10.1016/j.comptc.2012.06.011>
- [39] Janjua, M. R. S. A., et al., A DFT study on the two - dimensional second - order nonlinear optical (NLO) response of terpyridine - substituted hexamolybdates: physical insight on 2D inorganic–organic hybrid functional materials. 2012, Wiley Online Library. <http://dx.doi.org/10.1002/ejic.201101092>
- [40] Khan, M. U., et al., First theoretical probe for efficient enhancement of nonlinear optical properties of quinacridone based compounds through various modifications. 2019. 715: p. 222-230. <https://doi.org/10.1016/j.cplett.2018.11.051>
- [41] Khan, M. U., et al., Prediction of second-order nonlinear optical properties of D– π –A compounds containing novel fluorene derivatives: a promising route to giant hyperpolarizabilities. 2019. 30: p. 415-430. <https://link.springer.com/article/10.1007/s10876-018-01489-1>
- [42] Khan, M. U., et al., Designing star-shaped subphthalocyanine-based acceptor materials with promising photovoltaic parameters for non-fullerene solar cells. 2020. 5(36): p. 23039-23052. <https://doi.org/10.1021/acsomega.0c02766>
- [43] Hussain, R., et al., Enhancement in photovoltaic properties of N, N - diethylaniline based donor materials by bridging core modifications for efficient solar cells. 2020. 5(17): p. 5022-5034. <http://dx.doi.org/10.1002/slct.202000096>
- [44] Murray, J. S. and K. Sen, Molecular electrostatic potentials: concepts and applications. 1996.
- [45] Scrocco, E. and J. Tomasi, Electronic molecular structure, reactivity and intermolecular forces: an euristic interpretation by means of electrostatic molecular potentials, in Advances in quantum chemistry. 1978, Elsevier. p. 115-193. [https://doi.org/10.1016/S0065-3276\(08\)60236-1](https://doi.org/10.1016/S0065-3276(08)60236-1)
- [46] Thul, P., et al., Structural and spectroscopic studies on 2-pyranones. 2010. 75(1): p. 251-260. <https://doi.org/10.1016/j.saa.2009.10.020>